Front. Mech. Eng. 2023, 18(1): 18
https://doi.org/10.1007/s11465-022-0734-y

REVIEW ARTICLE

A review of low-temperature plasma-assisted machining: from mechanism to application

Jiyu LIU‡, Yuheng LI‡, Yang CHEN, Yuyang ZHOU, Shuaishuai WANG, Zizhen YUAN, Zhuji JIN, Xin LIU (✉)

Key Laboratory for Precision and Non-traditional Machining Technology of the Ministry of Education, Dalian University of Technology, Dalian 116024, China

✉ *Corresponding author. E-mail: xinliu@dlut.edu.cn (Xin LIU)*

ABSTRACT Materials with high hardness, strength or plasticity have been widely used in the fields of aviation, aerospace, and military, among others. However, the poor machinability of these materials leads to large cutting forces, high cutting temperatures, serious tool wear, and chip adhesion, which affect machining quality. Low-temperature plasma contains a variety of active particles and can effectively adjust material properties, including hardness, strength, ductility, and wettability, significantly improving material machinability. In this paper, we first discuss the mechanisms and applications of low-temperature plasma-assisted machining. After introducing the characteristics, classifications, and action mechanisms of the low-temperature plasma, we describe the effects of the low-temperature plasma on different machining processes of various difficult-to-cut materials. The low-temperature plasma can be classified as hot plasma and cold plasma according to the different equilibrium states. Hot plasma improves material machinability via the thermal softening effect induced by the high temperature, whereas the main mechanisms of the cold plasma can be summarized as chemical reactions to reduce material hardness, the hydrophilization effect to improve surface wettability, and the Rehbinder effect to promote fracture. In addition, hybrid machining methods combining the merits of the low-temperature plasma and other energy fields like ultrasonic vibration, liquid nitrogen, and minimum quantity lubrication are also described and analyzed. Finally, the promising development trends of low-temperature plasma-assisted machining are presented, which include more precise control of the heat-affected zone in hot plasma-assisted machining, cold plasma-assisted polishing of metal materials, and further investigations on the reaction mechanisms between the cold plasma and other materials.

KEYWORDS low-temperature plasma, difficult-to-cut material, machinability, hydrophilization effect, Rehbinder effect

1 Introduction

Titanium alloy, high temperature alloy, engineering ceramics, and other materials with superb properties have been widely used in special equipment, such as aero-engines, gas turbines, aircraft landing gear, nuclear main pumps, and seawater valves [1–10]. Although these materials generally have good mechanical strength and high ductility or hardness, they may also contain a variety of metal compounds and unevenly distributed hard particles, resulting in poor machinability [11–18]. During the machining process, problems such as high temperature, large cutting force, and serious tool wear are likely to occur, making it difficult to meet the increasingly high requirements of special service conditions for machining accuracy, surface integrity, and fatigue life [19].

To date, researchers have employed various cooling media to achieve the high-surface integrity machining of difficult-to-cut materials, including high-pressure coolant-assisted machining [20–22], liquid nitrogen-assisted machining [23,24], supercritical carbon dioxide-assisted machining [25–31], and minimum quantity lubrication (MQL)-assisted machining [32–36]. An et al. [25–31] creatively proposed supercritical CO_2-based MQL technology and applied the technique into materials, such

Received April 30, 2022; accepted August 22, 2022

‡ These authors contribute equally.

as carbon fiber-reinforced polymer composite material, TC4 titanium alloy, and graphite iron. Their results indicated that the hybrid cooling technology could effectively reduce cutting temperature, alleviate subsurface damage, and improve surface quality. Li et al. [33–35] innovatively combined compressed gas, degradable vegetable oil, and nanoparticles to improve the cooling and lubrication environments in the grinding area and found that the nanofluid MQL could significantly reduce specific grinding energy, avoid workpiece burn, and improve surface integrity. Apart from the cooling media, external energy fields, such as ultrasonic vibration, have also been applied to improve machinability [37–39]. For example, Bhaduri et al. [39] conducted ultrasonic vibration-assisted grinding experiments of γ-TiAl alloy and found that ultrasonic vibration could reduce grinding force and surface roughness *Ra* by ~35% and ~10%, respectively.

Although the abovementioned methods can reduce cutting temperature and cutting force, thus improving surface integrity, the material properties have not been changed. As a result, problems caused by the special mechanical strength, ductility, and hardness can still influence the machining process. At the same time, when surface temperature is higher than a certain value, a vapor layer will form when the cooling media are in contact with the surface due to the Leidenfrost effect, and the certain value obtained is called the "Leidenfrost temperature" [40,41]. The Leidenfrost effect leads to a significant decrease in solid–liquid contact area, making it difficult for the coolant to enter the cutting area for effective lubrication and cooling, resulting in relatively lower critical heat flux and heat transfer coefficient [42]. Therefore, it is of great significance to develop machining methods that can adjust material properties, so that material machinability can be effectively improved.

As a material state rich in active particles, plasma can effectively improve surface wettability as well as reduce material strength, hardness, and deformation resistance. When plasma is induced into a cutting area, its effects on material properties can effectively promote material fracture and the permeation of the cooling media into the cutting area, thus realizing the highly efficient, precise, and low-damage machining of difficult-to-cut materials. According to electron temperature T_e, plasma can be classified as high-temperature (T_e: ~10^8 K) and low-temperature plasma (T_e < 10^5 K). Compared with the high-temperature plasma, the low-temperature plasma is easier to obtain and maintain. In recent years, researchers have applied the latter into machining process, i.e., low-temperature plasma-assisted machining, which can significantly improve material machinability and surface integrity. However, the mechanisms, application ranges, and development trends of this promising technique have been rarely discussed. It should be of great significance to systematically discuss these issues, so as to provide enlightenments for further application and development of this technology. In this paper, after introducing basic characteristics of the low-temperature plasma, we expound the action mechanism of the low-temperature plasma-assisted machining, and then describe the application of the low-temperature plasma in the auxiliary processing of difficult-to-cut materials; finally, we prospect the development trend of the low-temperature plasma-assisted machining. Schematic diagram showing the overall structure of the paper is shown in Fig. 1.

2 Basic characteristics of low-temperature plasma and its mechanism in auxiliary machining

Plasma is an unbound macroscopic system consisting of charged particles and is generally regarded as the fourth state of matter after solid, liquid, and gas [43]. Plasma exists widely in nature, and more than 99% of matter in the universe, such as aurora, sun, and lightning, are in a plasma state. The classification of plasma according to the electron temperature T_e is shown in Table 1. On the one hand, T_e in the high-temperature plasma can reach 10^8 K, the plasma is completely ionized, and particle density is very high, which can be generated by the solar core in nature and tokamak devices in laboratories. On the other hand, T_e in the low-temperature plasma is lower than 10^5 K, the plasma is partially ionized, and it is generally generated by gas discharge in laboratories. Low-temperature plasma can be further divided into hot and cold plasma according to different thermodynamic equilibrium states [44,45]. Hot plasma is in a local thermodynamic equilibrium state, its T_e and ion temperature (T_i) are relatively high and approximately equal ($T_e \approx T_i$ in the range of 10^4–10^5 K), and the macroscopic temperature can reach up to 10^5 K. By contrast, cold plasma is in a non-local thermodynamic equilibrium state, the value of T_e (10^4–10^5 K) is much higher than T_i (10^3 K), and the macroscopic temperature is relatively low, even close to room temperature.

The schematic diagram and experimental setup of the low-temperature plasma-assisted machining process is shown in Fig. 2 [46,47]. The low-temperature plasma influences the machining process by physical and chemical effects. For hot plasma, the main effect is the thermal softening effect contributed by the high temperature. For cold plasma, the main mechanisms are reducing hardness, improving surface wettability, and promoting material fracture through chemical reactions. The mechanisms of the hot and cold plasma during the assisted machining process are summarized below.

Hot plasma: The high macroscopic temperature (> 10000 K) of hot plasma can effectively reduce mechanical strength and hardness of materials via the thermal softening effect. Thus, hot plasma can be applied in

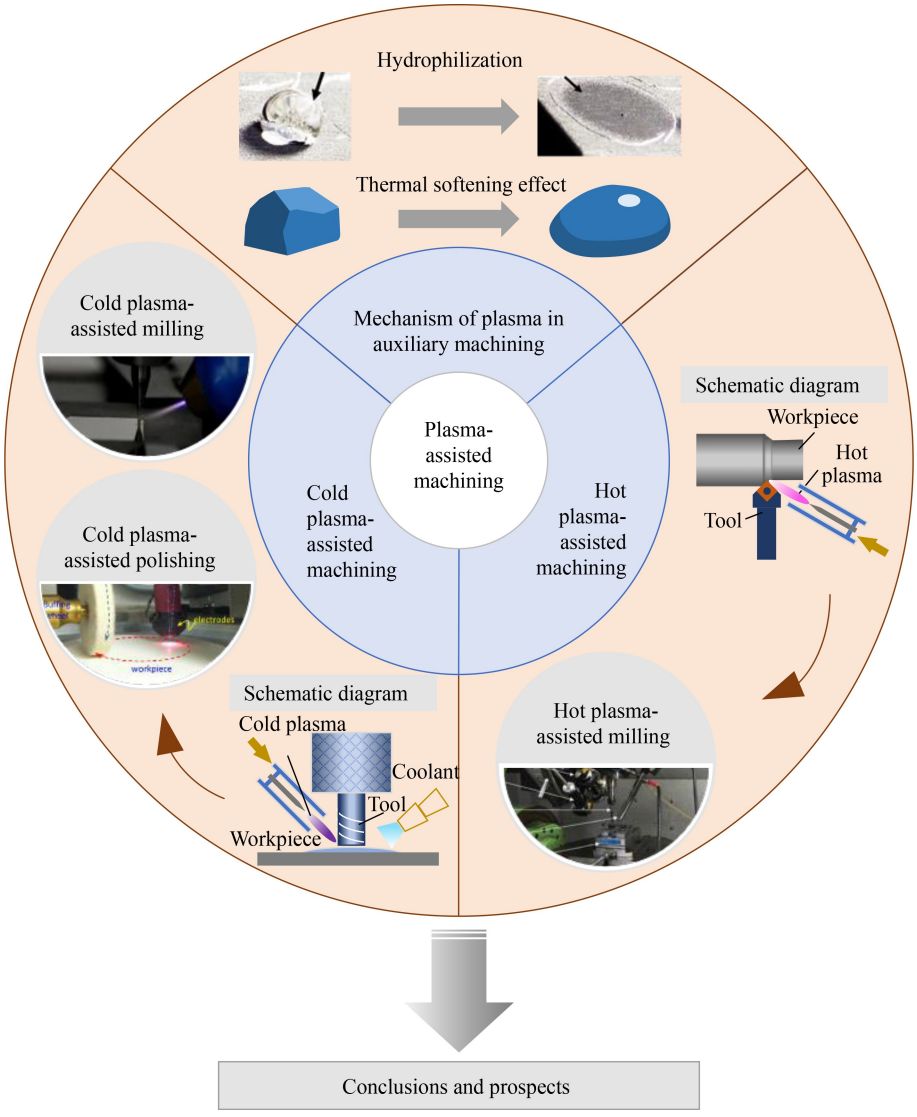

Fig. 1 Overall structure of the paper.

Table 1 Classification of plasma

Classification		Macroscopic temperature/K	Thermodynamic property	Examples
High-temperature plasma		10^6–10^8	Thermodynamic equilibrium	Solar core; thermonuclear fusion
Low-temperature plasma	Hot plasma	10^3–2×10^4	Local thermodynamic equilibrium	Arc plasma; high-frequency plasma; magnetic fluid discharge
	Cold plasma	300–500	Non-local thermodynamic equilibrium	Glow discharge; corona discharge; spark discharge

machining processes of high-strength and high-hardness materials, such as bearing steel, titanium alloy, and nickel-base superalloy (Figs. 2(a) and 2(b) [46]), thereby reducing cutting forces via the thermal softening effect, which ultimately improves material machinability. The mechanism of hot plasma-assisted machining (HPAM) has similarities with laser-assisted machining, which uses high-temperature plasma torch or laser beam to soften materials. Compared with laser-assisted machining, the use of hot plasma is relatively more economical, providing comparable heating rates at lower costs [48]. At the same time, the spot size of a plasma torch is larger, resulting in relatively lower heating accuracy, while also ensuring the heating of all radial cutting depths in the milling process [49,50].

Cold plasma: Although the macroscopic temperature of cold plasma is quite low, it contains a variety of high-energy active particles, including electrons (1–10 eV), excited atoms or molecules (0–20 eV), and photons (3–40 eV) [51]. The energies of these particles are generally

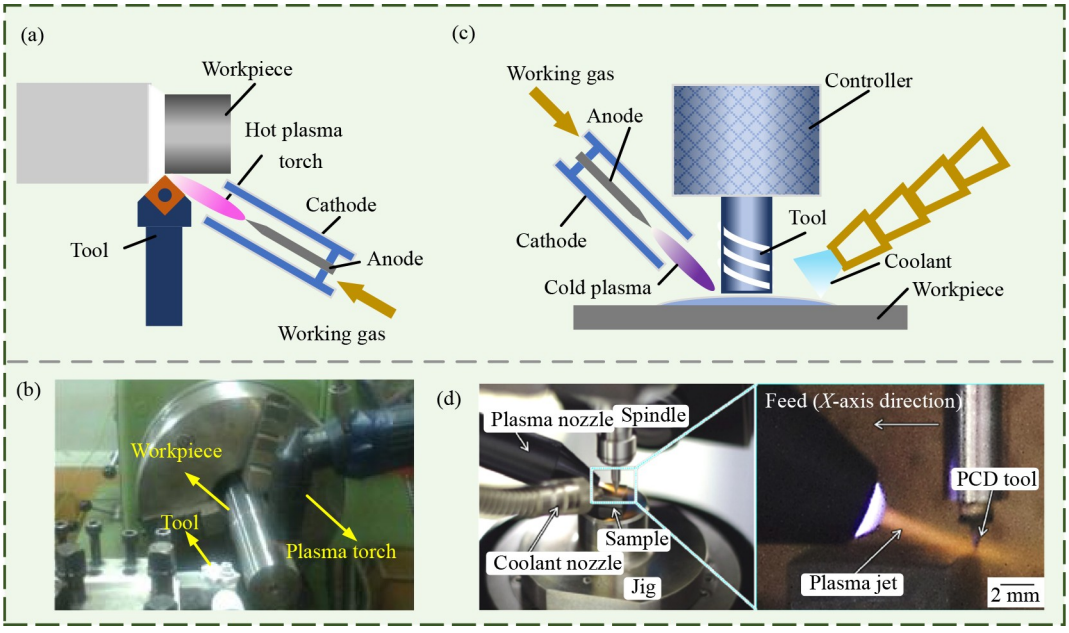

Fig. 2 Schematic diagram and experimental setup of the low-temperature plasma-assisted machining process: (a) schematic diagram and (b) experimental setup of hot plasma-assisted machining; (c) schematic diagram and (d) experimental setup of cold plasma-assisted machining. Reproduced with permissions from Refs. [46,47] from Taylor and Francis and Elsevier, respectively.

higher than those of typical chemical bonds, such as C–C (3.45 eV), C–F (4.69 eV), and C–H (4.3 eV). Therefore, when cold plasma is employed to treat materials, its active particles can break the chemical bonds of molecular chains; as dangling bonds appear at the broken positions, they generate free radicals. The active particles in cold plasma, such as O and OH, may combine with these free radicals and form hydrophilic oxygen-containing groups (e.g., C–O and C=O), thereby improving surface hydrophilicity. During the machining process of difficult-to-cut materials, the difficulties involved as coolants enter the cutting area as a result of the Leidenfrost effect contribute to the high cutting temperature and poor machinability [42]. Surfaces with better hydrophilicity have higher Leidenfrost temperature and heat transfer coefficient. Therefore, when cold plasma and other coolants are simultaneously induced into the cutting area (Figs. 2(c) and 2(d) [47]), the hydrophilization effect of the cold plasma may promote the coolants to permeate the cutting area, significantly improving the cooling and lubricating condition.

Aside from the effect in improving the permeability of coolants through hydrophilization, cold plasma may also reduce material strength and ductility due to the Rehbinder effect, which claims that active particles absorbing on cracks may promote crack propagation [52–54]. Cold plasma contains various active particles and may promote the expansion of cracks and lattice gaps. When applied into the machining process, cold plasma may reduce the ductility and deformation resistance of materials, effectively reducing cutting force, restraining tool wear, alleviating chip adhesion, and improving surface quality. When investigating the effects of cold plasma on these properties, surface wettability is generally characterized by measuring water contact angles. Meanwhile mechanical properties, such as ductility and deformation resistance, are characterized by nanoindentation measurement, single particle scratching test, and tensile experiment.

Cold plasma can effectively change surface properties without inducing obvious structural damage; thus, it has significant application values in other fields. For instance, radio frequency (RF) plasma-enhanced physical vapor deposition has been widely studied and applied in improving coating adhesion, i.e., the physical-chemical bonding between coatings and substrates [55–57]. Cold plasma can also be used for improving the painting ability [58] and corrosion resistance [59,60] of various materials.

According to the above discussion, with varying thermodynamic properties and macroscopic temperatures, the action mechanisms of hot plasma and cold plasma in assisted machining are radically different. The mechanism of hot plasma is the thermal softening effect, while that of cold plasma can be mainly attributed to chemical reactions. The different mechanisms contribute to the dissimilar applications of HPAM and cold plasma-assisted machining (CPAM), which are respectively described below.

3 Hot plasma-assisted machining

The demand for materials with high strength and good heat resistance has been increasing, particularly in

aerospace field. However, material properties, such as high strength and low thermal conductivity, bring about problems, including large cutting forces, high cutting temperatures, and serious tool wear. Given that the strain hardening rate and yield stress of materials significantly decrease with the increase of temperatures contributed by the thermal softening effect, thermally enhanced machining can effectively improve material machinability. Compared with flame heating and laser-assisted machining, HPAM has relatively higher heating efficiency and lower cost [48] and has been widely applied in the machining of difficult-to-cut materials.

During HPAM, most equipment adopts the plasma transferred arc, whose generating system is illustrated by the schematic diagram shown in Fig. 3. A hot plasma jet is first generated around the electrode by closing switch S_1; then, switch S_2 is closed to alter the electric circuit and form a plasma arc between the electrode and workpiece. The high temperature of the hot plasma requires large current (tens to hundreds of amperes) and a high power of thousands of watts [46,61]. The high temperature generated by the high power can effectively reduce material hardness through the thermal softening effect. As a result, less spindle power is required during machining, and higher productivity can be achieved [61].

Kitagawa et al. [62] first reported the HPAM technique for high-hardness metals, such as 18% Mn steel and 2.25% Cr cast iron. Their turning experiments indicated that the hot plasma could reduce cutting forces, alleviate flank wear, and improve surface roughness *Ra*. Madhavulu and Ahmed [61] applied hot plasma in the turning of stainless and alloy steels and revealed that the HPAM could improve material removal rate and tool life by 1.8 times and 1.67 times, respectively. López de Lacalle et al. [49] employed the HPAM to machine Haynes 25, Inconel 718, and Ti–6Al–4V, and found that cutting forces could be reduced by up to 25% while productivity was improved by 350% for the Haynes 25. For Inconel 718, the HPAM could significantly alleviate notch wear, thus contributing to the increase of ~200% in tool life. Lee et al. [50,63] developed an HPAM device (Fig. 4 [63]) and conducted HPAM experiments of Ti–6Al–4V, AISI 1045 steel, and Inconel 718. Their experimental results indicated that the surface roughness *Ra* and cutting force could be reduced by 70.5% and 60.2%, respectively, for Ti–6Al–4V [50]. Furthermore, when machining AISI 1045 steel, the HPAM decreased the cutting force by up to 61% and 15% compared with conventional machining and laser-assisted machining, respectively [63]. Farahnakian and Razfar [68] combined hot plasma and ultrasonic vibration to assist in the turning of hardened steel AISI 4140; compared with conventional turning (CT), the cutting force decreased by up to ~60%, and surface roughness *Ra* was improved by 5%–20%. Rao [48] investigated the hot plasma-assisted turning process of hardened AISI 4340 alloy steel and found that surface roughness *Ra* and tool wear were influenced by the heating temperatures of hot plasma and machining time. Under higher heating temperatures, the surface roughness *Ra* became relatively lower and increased more

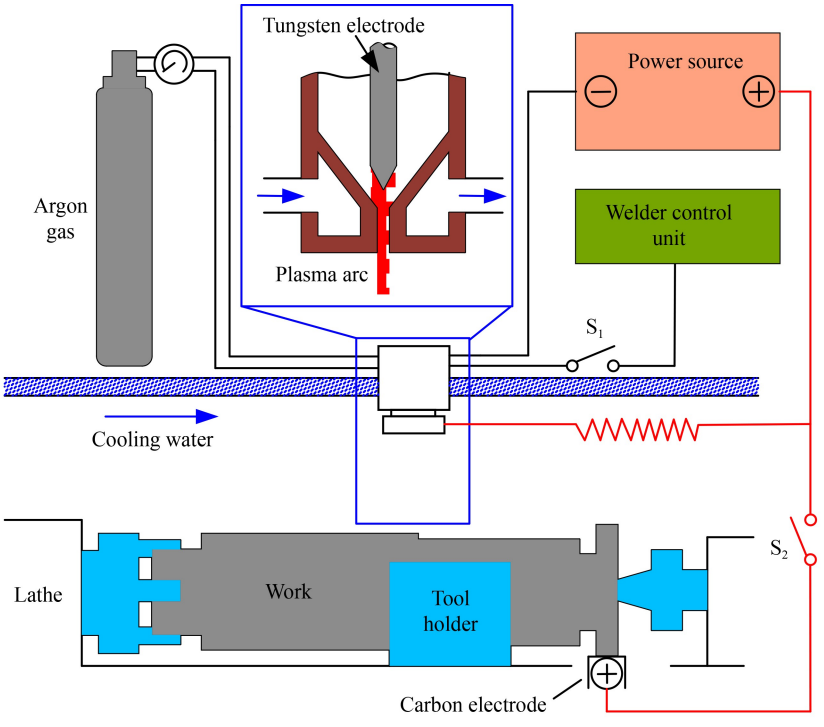

Fig. 3 Schematic diagram of the hot plasma generating system.

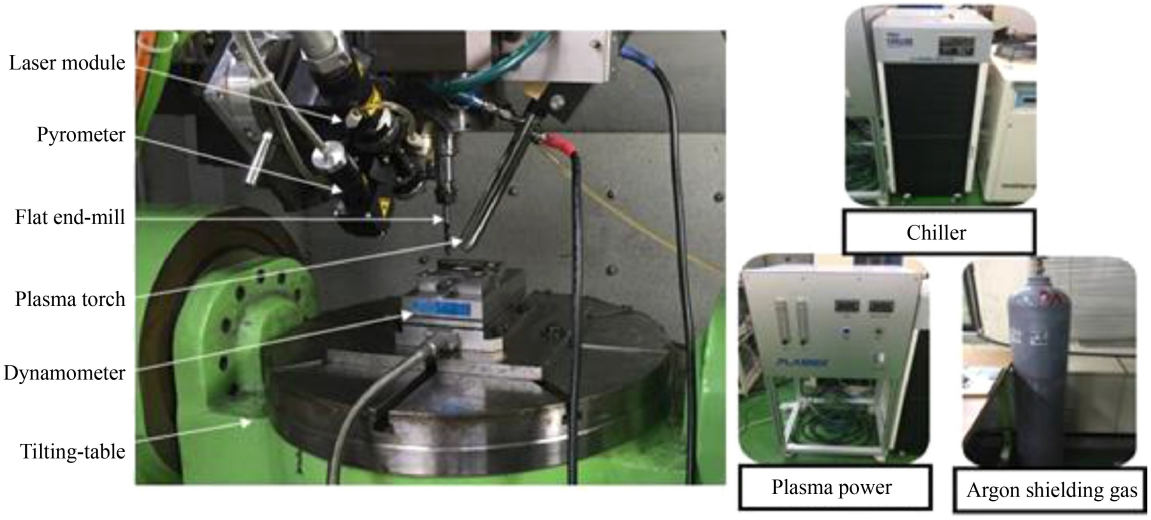

Fig. 4 Hot plasma-assisted machining device. Reproduced with permission from Ref. [63] from Elsevier.

slowly with the machining time (Fig. 5 [48]). They also found that tool wear form changed from notch wear to diffusion wear (873.15 K).

While hot plasma can reduce material strength and cutting forces by heating the cutting area, the heating effect may also cause an excessively high temperature of the cutting tools, leading to a serious reduction in tool life [46]. To reduce tool temperature and restrain groove wear, researchers have proposed a hybrid machining method combining hot plasma heating and liquid nitrogen cooling. Wang et al. [64] first employed the hybrid machining method to turn Inconel 718, in which the workpiece was heated by hot plasma, while the cutting tool was cooled by liquid nitrogen, as shown in Fig. 6(a) [64]. Experimental results demonstrated that the surface roughness *Ra* could be reduced by 250%, cutting forces were decreased by about 30%–50% (Fig. 6(b) [64]), and tool life was extended by 170% over CT. Feyzi and Safavi [65] employed hot plasma to soften the Inconel 718 workpiece; and simultaneously utilized liquid nitrogen to ensure that the tool insert was not overheated. Compared with conventional machining, tool flank wear was effectively alleviated, tool life improved by at least 4–8 times, and surface roughness *Ra* improved from 2.5 to 0.2 μm. Khani et al. [46] induced both hot plasma and liquid nitrogen into the turning process of 17-4PH stainless steel and found that the cutting force could be reduced by up to 48%. In addition, the tool flank wear decreased by 48%, and tool life improved by 117% thanks to the cooling of the cutting insert contributed by the liquid nitrogen (Fig. 7 [46]).

The experimental results of the HPAM indicate that the hot plasma can effectively improve material machinability. Apart from the machining experiments, researchers have also developed theoretical models depicting the HPAM process to further investigate the influence of hot plasma. Leshock et al. [66] systematically characterized

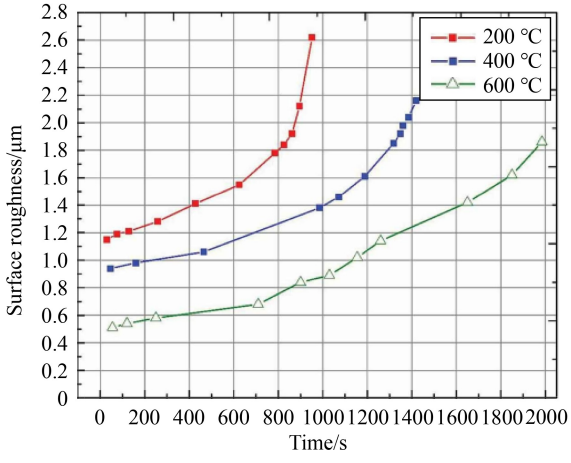

Fig. 5 Effect of heating temperature on surface roughness *Ra* with respect to the machining time. Reproduced with permission from Ref. [48] from Taylor and Francis.

the temperature distribution of the HPAM process of Inconel 718 through numerical modeling (Fig. 8 [66]) and experimental measurement, and the results of the numerical analysis and experimental investigation showed good agreement. HPAM experiments were then performed based on these analyses, and the results indicated that the plasma heating of the workpiece reduced resultant cutting forces by up to 30% and that specific shear energy of the HPAM was much lower. Meanwhile, the relatively higher chip temperature of the HPAM led to higher flank wear rates, whereas notch wear could be effectively alleviated and tool life was improved by 40%. Shao-Hsien and Tsai [67] conducted predictive analysis for the thermal diffusion of the HPAM process of Inconel 718 through exponential smoothing, and the exponential smoothing model was able to estimate cutting temperatures depending on plasma heating current and feed rate. Rao [48] established regression models for

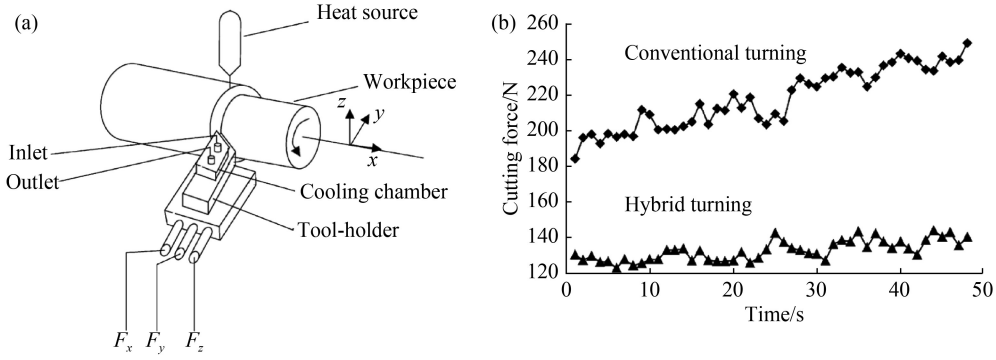

Fig. 6 Hybrid machining (combining hot plasma heating and liquid nitrogen cooling): (a) schematic of the experimental device and (b) main cutting force of conventional turning and hybrid turning. Reproduced with permission from Ref. [64] from Elsevier.

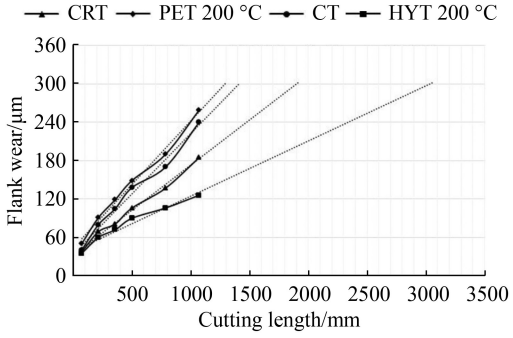

Fig. 7 Linear extrapolation of the flank wear for cryogenic liquid nitrogen turning (CRT), hot plasma-enhanced turning (PET), conventional turning (CT), and hybrid turning (HYT) combining CRT and PET. Reproduced with permission from Ref. [46] from Taylor and Francis.

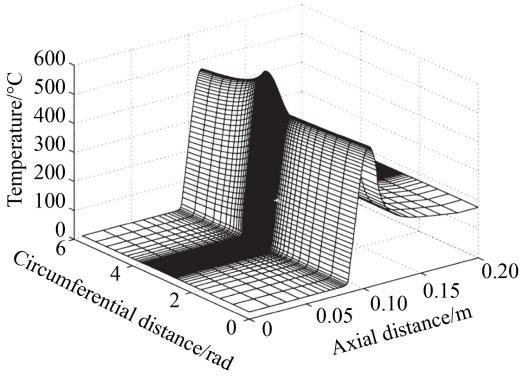

Fig. 8 Temperature distributions of the hot plasma-assisted machining process of the Inconel 718 cylinder surface. Reproduced with permission from Ref. [66] from Elsevier.

surface roughness *Ra*, tool wear, and material removal rate during the hot plasma-assisted turning process of AISI 4340 alloy steel, and the models could predict these measured values with accuracies all above 98%. The error between the predicated and experimental values were estimated to be 2.45%–9.22%, and the models could predict the surface roughness and tool life with a confidence interval of 99.8%. Moon and Lee [63] employed the ANSYS workbench thermal analysis software to predict preheating temperature distribution of the HPAM (Fig. 9 [63]) and found that the effective depth of cut was about 0.3 mm for AISI 1045 steel and 0.4 mm for Inconel 718.

Research results of the abovementioned experimental and theoretical work were generally consistent, demonstrating that the HPAM could effectively reduce cutting forces, extend tool life, and improve surface roughness *Ra* through the thermal softening effect, as listed in Table 2 [46,48–50,61–66]. The relatively optimal surface roughness *Ra* obtained by each work varied from ~0.1 to ~0.6 μm due to the differences in machining processes and workpieces materials, while they all showed significant improvement compared with conventional machining. However, the relatively large temperature gradient and limited controllability of the hot plasma heating may result in the excessively high temperature of the cutting area, leading to thermal damage and metamorphic layer of machined surfaces [49,68,69]. As shown in Fig. 10 [49], the hot plasma heating generated a metallurgical layer with Widmanstätten microstructures on the TC4 titanium alloy surface. The structure possessed higher hardness but poorer ductility, and its fatigue behavior was difficult to predict, which might restrain the application of machined surfaces. In addition, as it was difficult to precisely control the affected depth, there was still Widmanstätten microstructure after HPAM, as shown in Fig. 10(c). Therefore, the HPAM has been mostly applied in rough or semi-finishing machining of high-hardness or high-strength materials, while precision machining with low surface roughness (e.g., $Ra < 0.1$ μm) has been rarely reported with the use of HPAM.

4 Cold plasma-assisted machining

Compared with hot plasma, cold plasma has much lower macro temperature and is rich in active particles. Therefore, it can effectively adjust material properties,

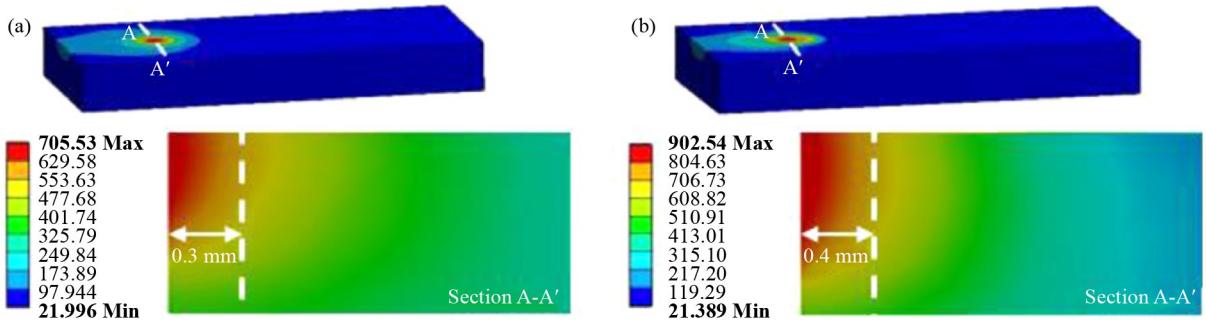

Fig. 9 Temperature distributions of the hot plasma-assisted machining processes of (a) AISI 1045 steel and (b) Inconel 718. Reproduced with permission from Ref. [63] from Elsevier.

Table 2 Summary of selected research papers that investigated HPAM

Workpiece materials	Authors	Machining process	Effects compared with conventional machining	Optimal surface roughness *Ra*
18% Mn steel, 2.25% Cr cast iron	Kitagawa et al. [62]	Turning	Decrease in cutting force, disappearance of built-up edge and chatter	Not mentioned
Stainless steel, alloy steel	Madhavulu and Ahmed [61]	Turning	1.8 times gain in material removal rate, 1.67 times improvement in tool life	Not mentioned
Inconel 718	Leshock et al. [66]	Turning	30% decrease in cutting force, 40% increase in tool life, two-fold improvement in *Ra*	~0.4 μm
Haynes 25, Inconel 718	López de Lacalle et al. [49]	Milling	25% decrease in cutting force and 350% increase in productivity for Haynes 25, 200% increase in tool life for Inconel 718	Not mentioned
Ti–6Al–4V	Lee and Lee [50]	Milling	60.2% decrease in cutting force, 70.5% improvement in *Ra*	0.111 μm
AISI 1045 steel, Inconel 718	Moon and Lee [63]	Milling	61% decrease in cutting force and 79% improvement in *Ra* for AISI 1045 steel, 57% decrease in cutting force and 82% improvement in *Ra* for Inconel 718	~0.1 μm for each material
Hardened AISI 4340 steel	Rao [48]	Turning	Tool wear form transferred from notch wear to flank wear, *Ra* was reduced	~0.5 μm
Inconel 718	Wang et al. [64]	Turning (with liquid N_2)	30%–50% decrease in cutting force, 250% reduction in *Ra*, 170% increase in tool life	~0.6 μm
Inconel 718	Feyzi and Safavi [65]	Turning (with liquid N_2, ultrasonic vibration)	4–8 times increase in tool life, 88%–93% improvement in *Ra*	~0.2 μm
17-4PH stainless steel	Khani et al. [46]	Turning (with liquid N_2)	48% reduction in cutting force, 48% decrease in tool flank wear, 18% improvement in *Ra*, 117% increase in tool life	~0.5 μm

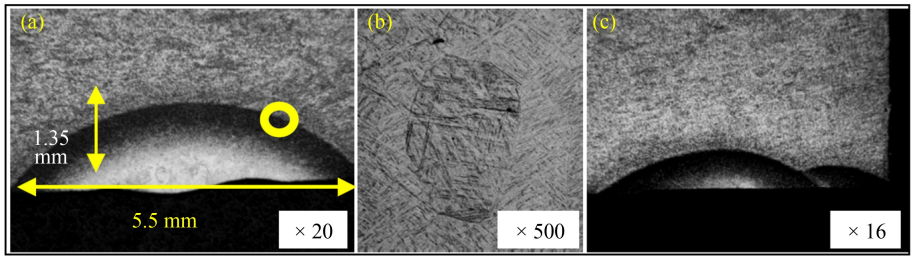

Fig. 10 Metallurgical microstructures induced by hot plasma heating: (a) heated zone, (b) Widmanstätten microstructure of the interface, and (c) affected zone after hot plasma-assisted machining. Reproduced with permission from Ref. [49] from ASME.

such as surface wettability and mechanical strength, without inducing obvious thermal damages [70–78]. Cold plasma can rapidly hydrophilize surfaces to be superhydrophilic (Fig. 11) and water can spread and penetrate more easily. Additionally, compared with hydrophilic or hydrophobic surfaces, the superhydrophilic surfaces can form larger liquid films under bubbles and has relatively higher Leidenfrost temperature, critical heat flux, and heat transfer coefficient [79–83]. Thus, when induced into the cutting area, cold plasma can effectively improve heat transfer efficiency of the coolants. Meanwhile, researchers have recently found that cold plasma can reduce material strength and hardness through chemical reactions [84] and the Rehbinder effect [85]. Currently, cold plasma has been applied into the machining processes of various materials. Given that the influence depth of cold plasma is quite limited, research on CPAM has mainly focused on precision machining.

Cold plasma is generally formed by gas discharge, and a typical system is shown in Fig. 12 [86]. As can be seen, working gas flowed through the pressure reducing valve and the flowmeter into the electrode, after which gas

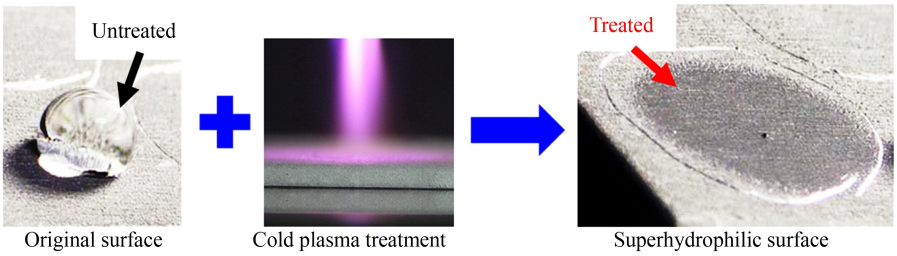

Fig. 11 Cold plasma hydrophilization process.

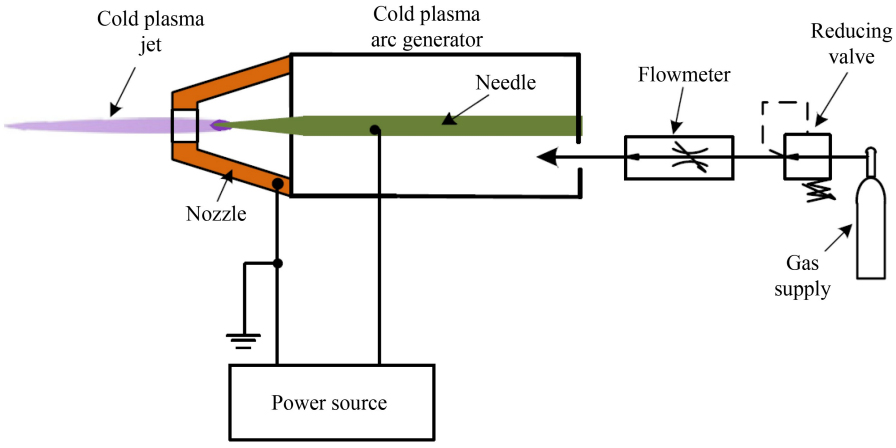

Fig. 12 Schematic diagram of the cold plasma-generating system. Reproduced with permission from Ref. [86] from Elsevier.

pressure and flow rate were respectively adjusted by the pressure reducing valve and the flowmeter. High voltage was applied between the needle and the nozzle to break down the working gas, thereby forming a cold plasma jet. Compared with hot plasma, with high voltage (kilovoltage level) but low current (milliampere level), the discharge power of cold plasma is quite low (can be even lower than 10 W [87,88]), the size of the generator is on the order of several hundred millimeters, and investment costs of the generator can be within 10000 USD. The relatively smaller sizes and lower costs of the cold plasma contribute to its promising application prospects.

4.1 Cold plasma-assisted polishing

The cold plasma-assisted polishing (CPAP) operates based on chemical reactions between the active particles in the cold plasma and material surfaces, so as to reduce material hardness, as well as improve material removal rate and surface integrity. Yamamura et al. [84] first proposed the CPAP technique, which reduced the hardness of hard materials through plasma irradiation, while polishing using soft abrasives (Fig. 13 [84]). In the past decade, they have applied the technique in processing a variety of materials, including silicon carbide [84,89–94], aluminum nitride [95,96], gallium nitride [97], and single-crystal diamonds [98–101]. The results demonstrated that cold plasma could oxidize the silicon carbide to turn it into silicon dioxide, leading to the significant decrease in hardness from 37.4 to 4.5 GPa [89]. The silicon dioxide could then be easily removed by hydrofluoric acid dipping or ceria abrasives (Fig. 14 [90]), and atomic flattening of the silicon carbide was achieved with a root mean square roughness of ~0.1 nm. When applying the CPAP into the aluminum nitride ceramic, the aluminum nitride was modified to be aluminum fluoride, and obvious improvements in surface integrity and material removal rate were achieved (Fig. 15 [95]). For single-crystal diamond, the cold plasma could convert the carbon atoms to carbon dioxide; thus, the material removal rate was 20 times greater than that of conventional polishing, and surface roughness *Sq* of 0.13 nm could be obtained [98]. Bastawros et al. [102] developed a CPAP platform (Fig. 16 [102]) and utilized atmospheric pressure He-H_2O plasma to assist the polishing of single crystal sapphire. The results indicated that the materials removal rate could be improved by two times, which can be attributed to the improvement of hydride formation on the sapphire surface by active chemical species. Lyu et al. [103] reported a novel polishing approach combining plasma treatment and low-pressure polishing for lutetium oxide. Their innovative polishing technique could obtain atomically smooth lutetium oxide surface with a surface roughness *Sa* of 0.47 nm.

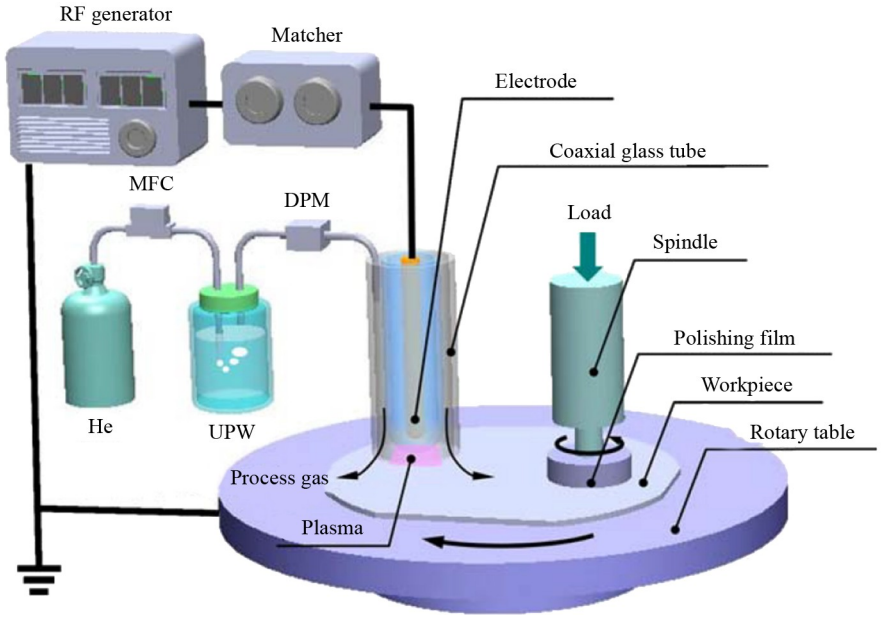

Fig. 13 Schematic diagram of the cold plasma-assisted polishing device. Reproduced with permission from Ref. [84] from Elsevier. RF: radio frequency, MFC: micro flow controller, DPM: dew-point meter, UPW: ultrapure water.

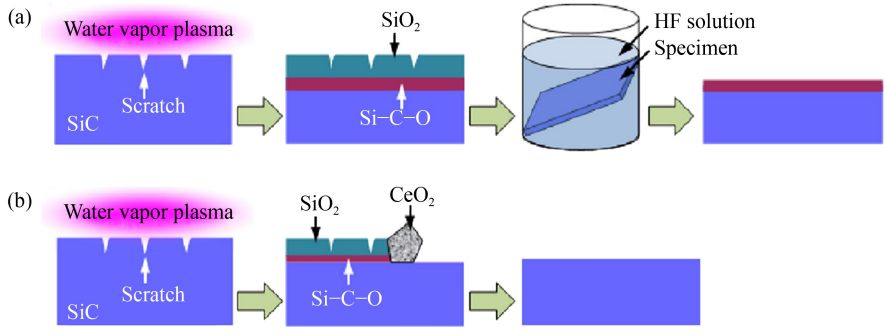

Fig. 14 Material removal mechanism of cold plasma-assisted polishing: (a) hydrofluoric acid dipping and (b) ceria abrasives. Reproduced with permission from Ref. [90] from Elsevier. HF: hydrofluoric acid.

The CPAP technology generates new compositions with relatively lower hardness through chemical reactions, thus reducing material hardness and significantly improving material removal rate and surface integrity. At present, the application of this technology mainly concentrates on non-metallic materials, such as silicon carbide and sapphire. Thus, the application of the CPAP in high-efficient and precision machining of engineering metal materials has great significance.

4.2 Cold plasma-assisted cutting

During the cold plasma-assisted cutting (CPAC) process, the movement speeds between the cutting tools and workpieces are relatively higher, and the tool-workpiece contact areas are smaller. Therefore, atmospheric pressure cold plasma jets (Fig. 17), which may more easily penetrate into the cutting area, have been widely used. Cold plasma jets were first reported by Koinuma et al. [104], who proposed a microbeam cold plasma-generating device to achieve the separation of discharge and treatment areas. Atmospheric pressure cold plasma jet could produce active particles in the surrounding air as well as eliminate the limitation of sample size caused by discharge devices [105–111]. In recent years, researchers have developed a variety of atmospheric pressure cold plasma jets [87,112–118], showing promising application prospects in the field of auxiliary cutting.

Liu et al. [119,120] first applied cold plasma jets in the machining of difficult-to-cut metal materials, such as NAK80 die steel and 304 stainless steel, as well as conducted surface wettability modification, friction and wear tests, and turning experiments. The results indicated that cold plasma jets could improve the surface wettability of metal materials and reduce friction coefficient between tool and friction pair, thus effectively reducing cutting forces, prolonging tool life, and improving surface quality. On this basis, Huang et al.

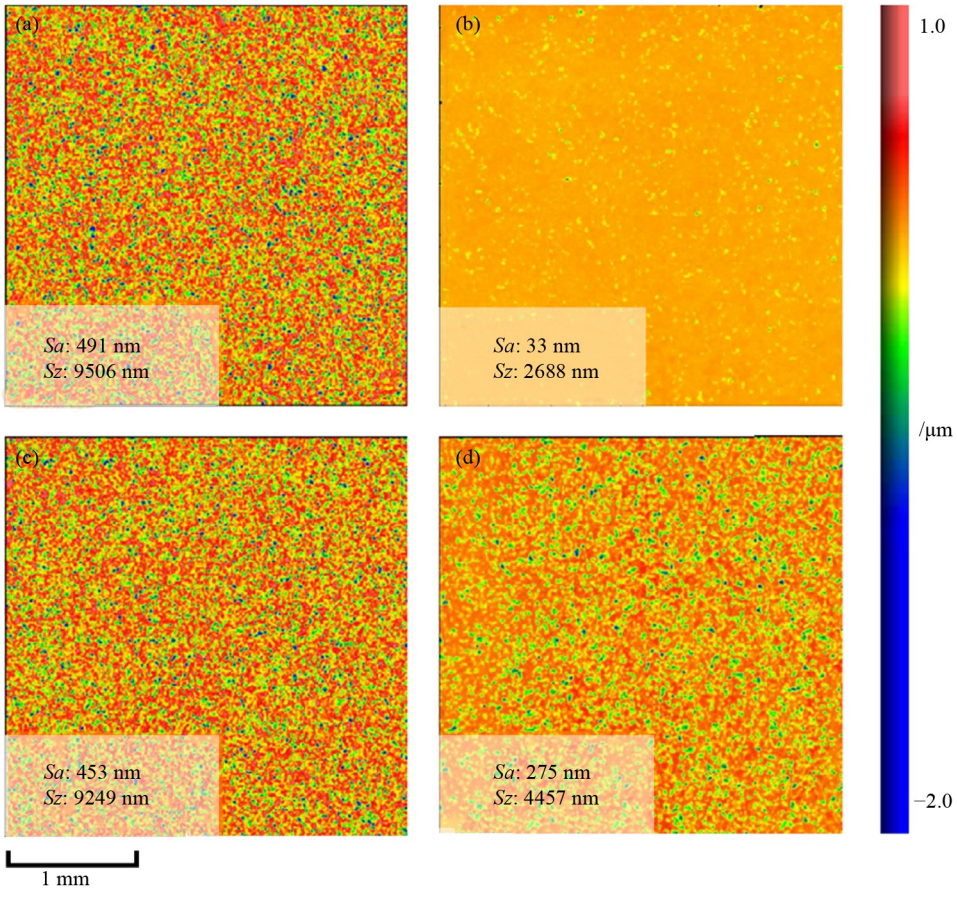

Fig. 15 Scanning white-light interferometer images of the aluminum nitride (a) before and (b) after plasma-assisted polishing, (c) before and (d) after conventional polishing. Reproduced with permission from Ref. [95] from Elsevier.

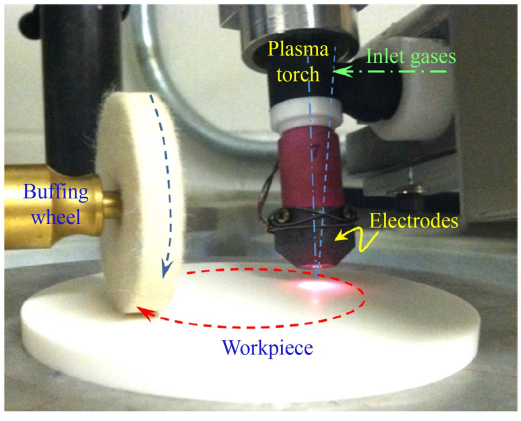

Fig. 16 Cold plasma-assisted polishing platform for single crystal sapphire. Reproduced with permission from Ref. [102] from Elsevier.

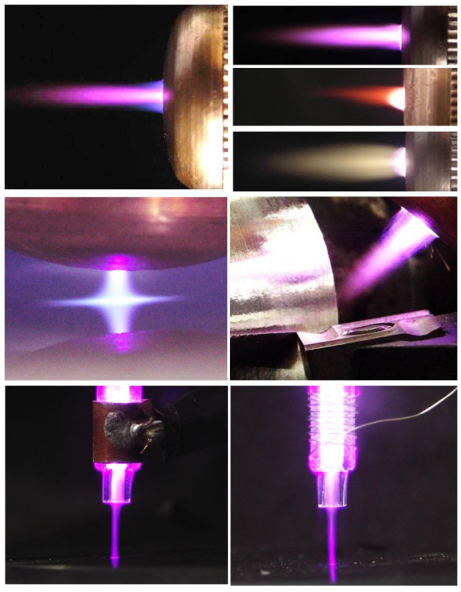

Fig. 17 Atmospheric pressure cold plasma jets.

[86,121,122] combined the cold plasma jet and ultrasonic elliptical vibration and proposed a hybrid turning (HYT) method for the diamond cutting of ferrous metals, as shown in Fig. 18 [121]. The ultrasonic vibration contributed to intermittent contact between the tool and workpiece, which promoted the cold plasma jet to enter the cutting area. Turning experiments demonstrated that the flank wear of the HYT was less than 50% of the CT, and surface roughness *Ra* was largely reduced. As coolants were not used in these experiments, the main

influence mechanisms of the cold plasma were the Rehbinder effect and chemical reactions induced by reactive particles. The Rehbinder effect contributed to the reduction in friction coefficient, and the chemical reactions formed nitrides, such as $Fe_xC_yN_x$, which inhibited graphitization of the diamond tool in cutting of ferrous metals [121].

The above CPAC methods could improve the machinability of various materials; however, these did not involve coolants, and the hydrophilization effect of the cold plasma jet was not utilized to adjust the cutting processes. Recently, Liu et al. [85,123–125] proposed a new hybrid machining method that combined the cold plasma jet and MQL, and applied the method in the turning, micro-grinding, and micro-milling processes of metal materials, including pure iron, GCr15 bearing steel, TC4 titanium alloy, and Inconel 718 superalloy, as shown in Fig. 19 [125]. The machining experiments indicated that the hybrid machining method could obviously reduce cutting temperatures and cutting forces, alleviate tool wear, and improve surface integrity. For the TC4 titanium alloy, compared with dry micro-milling, the main cutting force was reduced by 25%, surface roughness *Ra* was improved by 50%, and cracks on the machined surface could be obviously alleviated (Fig. 20 [85]). The cold plasma jet rapidly improved surface wettability without inducing obvious structural damages, thereby facilitating permeation of the MQL coolant into the cutting area. In addition, the cold plasma jet promoted material fracture due to the Rehbinder effect, which led to the decrease of cutting forces and alleviation of cracks on the machined surface.

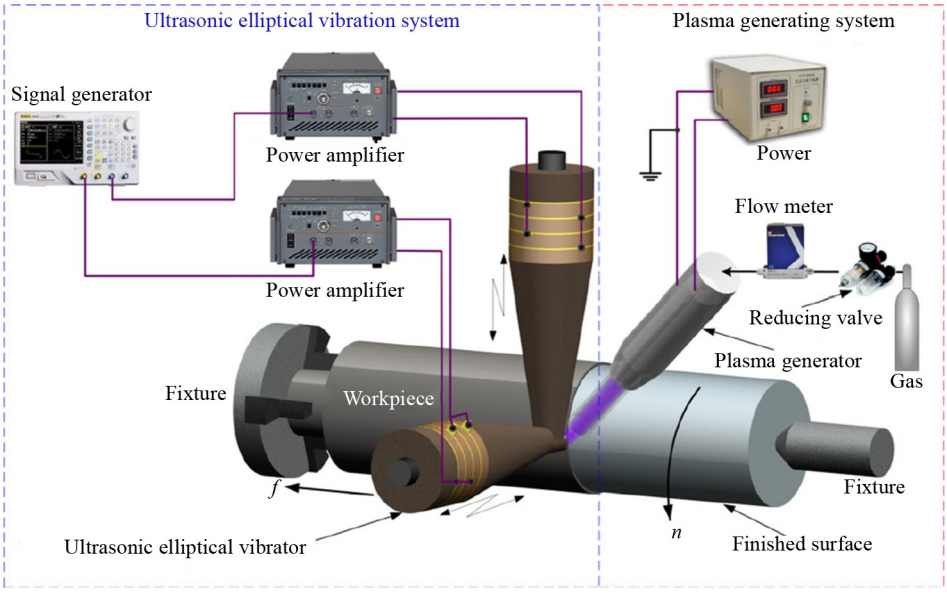

Fig. 18 Schematic diagram of the hybrid turning process (combining the cold plasma jet and ultrasonic elliptical vibration). Reproduced with permission from Ref. [121] from Springer Nature.

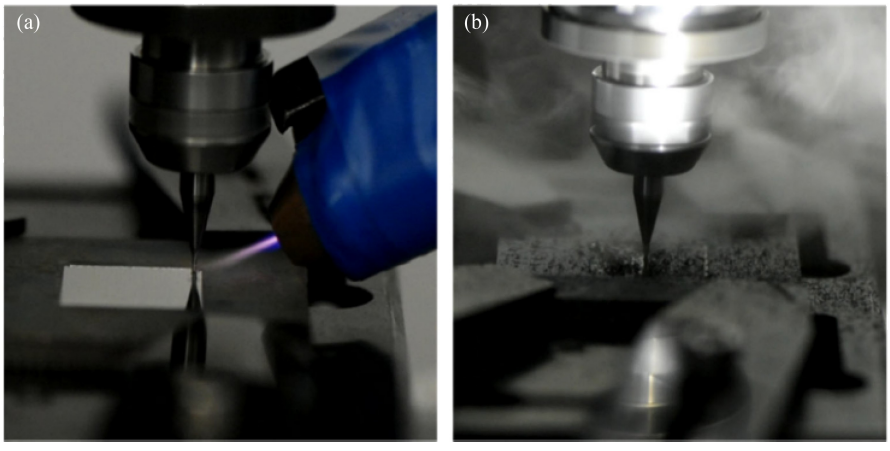

Fig. 19 Machining process of Inconel 718: (a) cold plasma-assisted micro-milling and (b) minimum quantity lubrication-assisted micro-milling. Reproduced with permission from Ref. [125] from Springer Nature.

Katahira et al. [47] investigated the cold plasma jet-assisted micro-milling of silicon carbide and found that the cold plasma jet obviously reduced surface roughness *Ra* and improve surface quality. During the CPAC process, the relatively optimum *Ra* reached ~0.73 nm and remained around 1–2 nm after micro-milling for 3000 mm. By contrast, for the conventional micro-milling, the *Ra* gradually increased from ~3 to ~6 nm with the increase of cutting distance. According to their investigation on the influence mechanism of the cold plasma jet, the plasma treatment led to better hydrophilicity by generating silicon dioxide layers on the silicon carbide surface. Thus, coolants could more easily permeate into the cutting area (Fig. 21 [47]), which contributed to the improvements of cooling and lubrication environment, surface quality, and tool life.

The CPAC technique effectively improved material machinability via the hydrophilization effect, chemical reactions, and the Rehbinder effect induced by the cold plasma jet. It should be of great importance to investigate the reaction mechanisms between the active particles in the cold plasma jet and material surfaces. Meanwhile, for the machining processes under higher temperature and more severe lubrication conditions, such as grinding, techniques to ensure the plasma jet can break through the air barriers remain to be further studied.

In summary, cold plasma could achieve low-damage and high-precision machining of various materials, as listed in Table 3 [47,84–86,89–102,119,121,122,124]. For the CPAP of non-metallic materials, such as silicon carbide and single-crystal diamonds, the main mechanism involved the chemical reactions between the cold plasma and the materials reduced material hardness. By contrast, the machining mechanism of CPAC was attributed to the hydrophilization and Rehbinder effects.

While the mechanisms of the CPAM have been studied and attributed to chemical reactions and the Rehbinder effect, the influences of these reactions on material properties still require further investigation. When the hot plasma is applied in auxiliary machining, the main

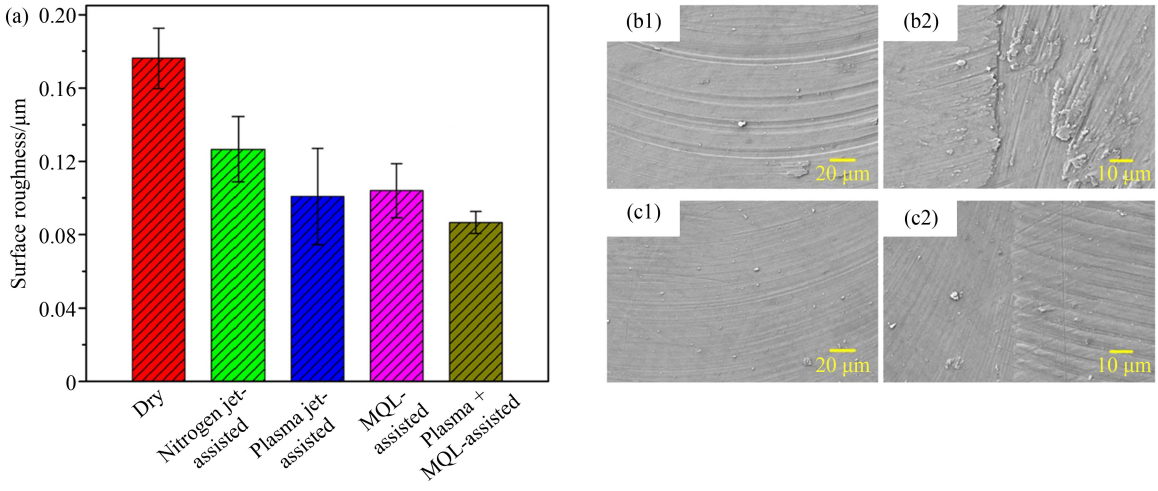

Fig. 20 Surface quality of Ti–6Al–4V machined by different micro-milling methods: (a) surface roughness *Ra*; scanning electron microscope images of (b1) surface microstructure and (b2) tool mark obtained by dry micro-milling; (c1) surface microstructure and (c2) tool mark obtained by cold plasma + minimum quantity lubrication (MQL)-assisted micro-milling. Reproduced with permission from Ref. [85] from Springer Nature.

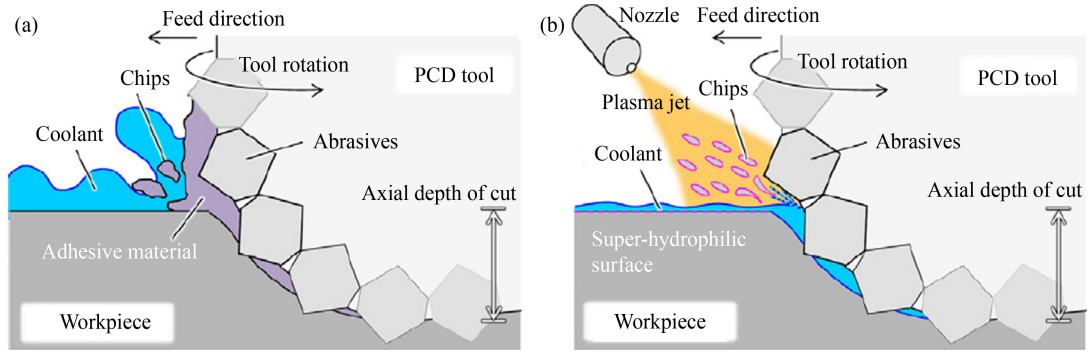

Fig. 21 Schematic diagrams illustrating the influence mechanism of the cold plasma jet on tool-workpiece interface: (a) without plasma jet and (b) with plasma jet. Reproduced from Ref. [47] with permission from Elsevier. PCD: polycrystalline diamond.

Table 3 Summary of selected research papers in CPAM

Workpiece material	Reference	Machining process	Effects compared with conventional machining	Optimal surface roughness
Silicon carbide	Yamamura et al. [84,89–94]	Polishing	Decrease in hardness from 37.4 to 4.5 GPa, achieving atomic flattening	RMS: ~0.1 nm
Aluminum nitride	Sun et al. [95,96]	Polishing	2 times gain in material removal rate, improvement in surface quality	*Sa*: ~3 nm
Gallium nitride	Deng et al. [97]	Polishing	Decrease in hardness from 22.7 to 13.9 GPa	*Sq*: ~0.1 nm
Single-crystal diamond	Yamamura et al. [98–101]	Polishing	20 times gain in material removal rate	*Sq*: ~0.13 nm
Single-crystal sapphire	Bastawros et al. [102]	Polishing	2 times improvement in material removal rate	*Sq*: ~0.23 μm
304 stainless steel	Liu [119]	Turning	13%–17% reduction in cutting forces, 69% decrease in flank wear	Not mentioned
NAK80 die steel	Huang et al. [86,121,122]	Turning (with ultrasonic vibration)	50% decrease in flank wear	*Ra*: ~1.5 μm
Ti–6Al–4V	Liu et al. [85]	Micro-milling (with MQL)	25% reduction in main cutting force, 50% improvement in *Ra*, alleviation of cracks on machined surfaces	*Ra*: ~0.08 μm
Silicon carbide	Katahira et al. [47]	Micro-milling	Significant improvements in surface quality and tool life	*Ra*: ~0.73 nm
GCr15	Liu et al. [124]	Micro-grinding (with MQL)	82% reduction in main cutting force, 65% improvement in *Ra*, alleviation of chip adhesion	*Ra*: ~0.23 μm

Note. RMS: root mean square.

mechanisms for different materials are indeed similar, i.e., reducing material hardness and strength via the thermal softening effect. By contrast, for the cold plasma, its influence on properties of various materials can vary widely. Therefore, it is promising to conduct experimental research and molecular dynamic simulation to further reveal the influence mechanisms of cold plasma on material properties, which are expected to largely facilitate the further application of CPAM in the future. In addition, the Rehbinder effect is mainly concerned about the interaction between reactive particles and crystal materials. For non-crystal brittle materials, the influences of cold plasma on mechanical properties and minimum chip thickness also require further investigation.

5 Conclusions

Materials with high hardness, strength, or plasticity have been widely used in aviation, aerospace, military, and other fields, but the machinability of these materials is generally poor. These lead to problems, such as large cutting forces, high cutting temperatures, serious tool wear, and chip adhesions, which seriously affect machining quality. Low-temperature plasma, which contains a variety of active particles, could effectively improve material machinability and has been widely applied in auxiliary machining process of difficult-to-cut materials. However, the mechanisms, applications, and development prospects of this promising technique have been rarely discussed in the literature. In this paper, after introducing the basic characteristics, classifications, and action mechanisms of low-temperature plasma, we respectively discussed the influence mechanisms, machining accuracy, and applications of HPAM and CPAM. The main conclusions and prospects are summarized as follows:

(1) According to the different thermodynamic equilibrium states, low-temperature plasma can be classified as hot plasma and cold plasma corresponding to different macroscopic temperatures. Under a local thermodynamic equilibrium state, the macroscopic temperature of hot plasma is higher than the melting points of most materials, and it can improve material machinability via the thermal softening effect. By contrast, cold plasma is under a non-local thermodynamic equilibrium state with a macroscopic temperature that is close to room temperature. The main mechanisms of CPAM can be attributed to the chemical reactions that reduce material hardness, improve surface wettability, and promote fracture.

(2) Hot plasma can reduce material hardness and strength through the thermal softening effect, thus contributing to the decrease in cutting force, the extension of tool life, and the improvement in surface quality. The relatively optimal surface roughness *Ra* varied from ~0.1 to ~0.6 μm for different workpiece materials, showing significant improvement compared with conventional machining. However, the relatively large temperature gradient and limited controllability of hot plasma heating may result in thermal damage and thermal stress. Therefore, HPAM has been mostly used in semi-precision and rough machining of difficult-to-cut materials with high hardness or strength. It may be promising to develop methods to better control the heat-affected zones by experimental research and thermal analysis, which can help achieve low-damage and high-efficient machining.

(3) With low macroscopic temperature, cold plasma can realize rapid surface modification without changing surface microstructures or textures. During the machining process, cold plasma can effectively reduce material hardness or improve surface wettability through the chemical reactions between the active particles and material surfaces, as well as promote material fracture of metal materials via the Rehbinder effect. On this basis, cold plasma has been applied into precision machining of

various materials, including polishing of non-metallic materials like silicon carbide, as well as the turning, micro-milling, and micro-grinding of metal materials, such as die steel and titanium alloy. In future works, it should be of great significance to focus on high-efficient and high-integrity polishing of metal materials. It may also be a promising research direction to investigate the effects of the cold plasma on mechanical properties and minimum chip thickness of non-crystal brittle materials. In addition, further investigations into the influence mechanisms of cold plasma on material properties may also be conducted through experiments and molecular dynamic simulations, as these can significantly facilitate the other applications of cold plasma in the future.

Nomenclature

CPAC	Cold plasma-assisted cutting
CPAM	Cold plasma-assisted machining
CPAP	Cold plasma-assisted polishing
CRT	Cryogenic liquid nitrogen turning
CT	Conventional turning
DPM	Dew-point meter
HF	Hydrofluoric acid
HPAM	Hot plasma-assisted machining
HYT	Hybrid turning
MFC	Micro flow controller
MQL	Minimum quantity lubrication
PCD	Polycrystalline diamond
PET	Plasma-enhanced turning
RF	Radio frequency
RMS	Root mean square
UPW	Ultrapure water

Acknowledgements This work was supported by the National Natural Science Foundation of China (Grant No. 51975092) and the Fundamental Research Funds for the Central Universities, China (Grant No. DUT19ZD202). The authors sincerely thank the researchers and original publishers for granting permission to use the figures included in this paper.

References

1. Bai H Q, Zhong L S, Kang L, Liu J B, Zhuang W J, Lv Z L, Xu Y H. A review on wear-resistant coating with high hardness and high toughness on the surface of titanium alloy. Journal of Alloys and Compounds, 2021, 882: 160645
2. Heimann R B. Silicon nitride, a close to ideal ceramic material for medical application. Ceramics, 2021, 4(2): 208–223
3. Balbus G H, Kappacher J, Sprouster D J, Wang F L, Shin J, Eggeler Y M, Rupert T J, Trelewicz J R, Kiener D, Maier-Kiener V, Gianola D S. Disordered interfaces enable high temperature thermal stability and strength in a nanocrystalline aluminum alloy. Acta Materialia, 2021, 215: 116973
4. Pollock T M. Alloy design for aircraft engines. Nature Materials, 2016, 15(8): 809–815
5. Veiga C, Davim J P, Loureiro A J R. Review on machinability of titanium alloys: the process perspective. Reviews on Advanced Materials Science, 2013, 34(2): 148–164
6. Davim J P. Mechanical and Industrial Engineering: Historical Aspects and Future Directions. Cham: Springer, 2022
7. Davim J P. Machining of Titanium Alloys. Heidelberg: Springer, 2014
8. Ma D X. Novel casting processes for single-crystal turbine blades of superalloys. Frontiers of Mechanical Engineering, 2018, 13(1): 3–16
9. Khanna N, Davim J P. Design-of-experiments application in machining titanium alloys for aerospace structural components. Measurement, 2015, 61: 280–290
10. Hu D Y, Wang X Y, Mao J X, Wang R Q. Creep-fatigue crack growth behavior in GH4169 superalloy. Frontiers of Mechanical Engineering, 2019, 14(3): 369–376
11. Wang X Y, Huang C Z, Zou B, Liu G L, Zhu H T, Wang J. Experimental study of surface integrity and fatigue life in the face milling of Inconel 718. Frontiers of Mechanical Engineering, 2018, 13(2): 243–250
12. Sun T, Qin L F, Hou J M, Fu Y C. Machinability of damage-tolerant titanium alloy in orthogonal turn-milling. Frontiers of Mechanical Engineering, 2020, 15(3): 504–515
13. Pimenov D Y, Mia M, Gupta M K, Machado A R, Tomaz Í V, Sarikaya M, Wojciechowski S, Mikolajczyk T, Kapłonek W. Improvement of machinability of Ti and its alloys using cooling-lubrication techniques: a review and future prospect. Journal of Materials Research and Technology, 2021, 11: 719–753
14. Li G X, Chandra S, Rahman Rashid R A, Palanisamy S, Ding S L. Machinability of additively manufactured titanium alloys: a comprehensive review. Journal of Manufacturing Processes, 2022, 75: 72–99
15. Sarikaya M, Gupta M K, Tomaz I, Danish M, Mia M, Rubaiee S, Jamil M, Pimenov D Y, Khanna N. Cooling techniques to improve the machinability and sustainability of light-weight alloys: a state-of-the-art review. Journal of Manufacturing Processes, 2021, 62: 179–201
16. Davim J P. Machining: Fundamentals and Recent Advances. London: Springer, 2008

17. Lauro C H, Filho S L M R, Brandão L C, Davim J P. Analysis of behaviour biocompatible titanium alloy (Ti–6Al–7Nb) in the micro-cutting. Measurement, 2016, 93: 529–540
18. Davim J P. Nontraditional Machining Processes: Research Advances. London: Springer, 2013
19. Yao Z Q, Fan C, Zhang Z, Zhang D H, Luo M. Position-varying surface roughness prediction method considering compensated acceleration in milling of thin-walled workpiece. Frontiers of Mechanical Engineering, 2021, 16(4): 855–867
20. Vijaya Ganesa Velan M, Subha Shree M, Muthuswamy P. Effect of cutting parameters and high-pressure coolant on forces, surface roughness and tool life in turning AISI 1045 steel. Materials Today: Proceedings, 2021, 43: 482–489
21. Díaz-Álvarez A, Díaz-Álvarez J, Cantero J L, Miguélez M H. High-pressure cooling in finishing turning of Haynes 282 using carbide tools: Haynes 282 and Inconel 718 comparison. Metals, 2021, 11(12): 1916
22. Ayed Y, Germain G. High-pressure water-jet-assisted machining of Ti555-3 titanium alloy: investigation of tool wear mechanisms. The International Journal of Advanced Manufacturing Technology, 2018, 96(1–4): 845–856
23. Wang F B, Wang Y Q. Comparison of cryogenic cooling strategy effects on machinability of milling nickel-based alloy. Journal of Manufacturing Processes, 2021, 66: 623–635
24. Gupta M K, Song Q H, Liu Z Q, Sarikaya M, Mia M, Jamil M, Singla A K, Bansal A, Pimenov D Y, Kuntoğlu M. Tribological performance based machinability investigations in cryogenic cooling assisted turning of α-β titanium alloy. Tribology International, 2021, 160: 107032
25. Tu L Q, Chen J, An Q L, Ming W, Xu J Y, Chen M, Lin L, Yang Z M. Machinability improvement of compacted graphite irons in milling process with supercritical CO_2-based MQL. Journal of Manufacturing Processes, 2021, 68: 154–168
26. Yu W, Chen J, Ming W, An Q L, Chen M. Feasibility of supercritical CO_2-based minimum quantity lubrication to improve the surface integrity of 50% Sip/Al composites. Journal of Manufacturing Processes, 2022, 73: 364–374
27. Dang J Q, Zang H, An Q L, Ming W, Chen M. Feasibility study of creep feed grinding of 300M steel with zirconium corundum wheel. Chinese Journal of Aeronautics, 2022, 35(3): 565–578
28. Dang J Q, Zhang H, An Q L, Ming W, Chen M. On the microstructural evolution pattern of 300M steel subjected to surface cryogenic grinding treatment. Journal of Manufacturing Processes, 2021, 68: 169–185
29. Zou F, Zhong B F, Zhang H, An Q L, Chen M. Machinability and surface quality during milling CFRP laminates under dry and supercritical CO_2-based cryogenic conditions. International Journal of Precision Engineering and Manufacturing—Green Technology, 2022, 9(3): 765–781
30. An Q L, Cai C Y, Zou F, Liang X, Chen M. Tool wear and machined surface characteristics in side milling Ti6Al4V under dry and supercritical CO_2 with MQL conditions. Tribology International, 2020, 151: 106511
31. Dang J Q, Zhang H, An Q L, Ming W, Chen M. Surface modification of ultrahigh strength 300M steel under supercritical carbon dioxide ($scCO_2$)-assisted grinding process. Journal of Manufacturing Processes, 2021, 61: 1–14
32. Liu M Z, Li C H, Zhang Y B, An Q L, Yang M, Gao T, Mao C, Liu B, Cao H J, Xu X F, Said Z, Debnath S, Jamil M, Ali H M, Sharma S. Cryogenic minimum quantity lubrication machining: from mechanism to application. Frontiers of Mechanical Engineering, 2021, 16(4): 649–697
33. Wang X M, Li C H, Zhang Y B, Said Z, Debnath S, Sharma S, Yang M, Gao T. Influence of texture shape and arrangement on nanofluid minimum quantity lubrication turning. The International Journal of Advanced Manufacturing Technology, 2022, 119(1–2): 631–646
34. Yang M, Li C H, Zhang Y B, Jia D Z, Zhang X P, Hou Y L, Li R Z, Wang J. Maximum undeformed equivalent chip thickness for ductile-brittle transition of zirconia ceramics under different lubrication conditions. International Journal of Machine Tools and Manufacture, 2017, 122: 55–65
35. Guo S M, Li C H, Zhang Y B, Wang Y G, Li B K, Yang M, Zhang X P, Liu G T. Experimental evaluation of the lubrication performance of mixtures of castor oil with other vegetable oils in MQL grinding of nickel-based alloy. Journal of Cleaner Production, 2017, 140: 1060–1076
36. Gupta M K, Boy M, Korkmaz M E, Yaşar N, Günay M, Krolczyk G M. Measurement and analysis of machining induced tribological characteristics in dual jet minimum quantity lubrication assisted turning of duplex stainless steel. Measurement, 2022, 187: 110353
37. Wang Y D, Kang R K, Qin Y, Meng Q, Dong Z G. Effects of inclination angles of disc cutter on machining quality of Nomex honeycomb core in ultrasonic cutting. Frontiers of Mechanical Engineering, 2021, 16(2): 285–297
38. Zhou W H, Tang J Y, Shao W. Modelling of surface texture and parameters matching considering the interaction of multiple rotation cycles in ultrasonic assisted grinding. International Journal of Mechanical Sciences, 2020, 166: 105246
39. Bhaduri D, Soo S L, Aspinwall D K, Novovic D, Bohr S, Harden P, Webster J A. Ultrasonic assisted creep feed grinding of gamma titanium aluminide using conventional and superabrasive wheels. CIRP Annals-Manufacturing Technology, 2017, 66(1): 341–344
40. Bourrianne P, Lv C J, Quéré D. The cold Leidenfrost regime. Science Advances, 2019, 5(6): eaaw0304
41. Quéré D. Leidenfrost dynamics. Annual Review of Fluid Mechanics, 2013, 45(1): 197–215
42. Alagan N T, Hoier P, Beno T, Klement U, Wretland A. Coolant boiling and cavitation wear—a new tool wear mechanism on WC tools in machining alloy 718 with high-pressure coolant. Wear, 2020, 452–453: 203284
43. Levchenko I, Xu S Y, Baranov O, Bazaka O, Ivanova E, Bazaka K. Plasma and polymers: recent progress and trends. Molecules, 2021, 26(13): 4091
44. Huang Y W, Yu Q F, Li M, Sun S N, Zhao H, Jin S X, Fan J, Wang J G. An overview of low-temperature plasma surface modification of carbon materials for removal of pollutants from liquid and gas phases. Plasma Processes and Polymers, 2021, 18(3): 2000171
45. Vajpayee M, Singh M, Ledwani L. Non-thermal plasma treatment of cellulosic biopolymer to enhance its surface property for

various applications: a review. Materials Today: Proceedings, 2021, 43: 3250–3255
46. Khani S, Farahnakian M, Razfar M R. Experimental study on hybrid cryogenic and plasma-enhanced turning of 17-4PH stainless steel. Materials and Manufacturing Processes, 2015, 30(7): 868–874
47. Katahira K, Ohmori H, Takesue S, Komotori J, Yamazaki K. Effect of atmospheric-pressure plasma jet on polycrystalline diamond micro-milling of silicon carbide. CIRP Annals-Manufacturing Technology, 2015, 64(1): 129–132
48. Rao T B. Reliability analysis of the cutting tool in plasma-assisted turning and prediction of machining characteristics. Australian Journal of Mechanical Engineering, 2022, 20(4): 1020–1034
49. López de Lacalle L N, Sánchez J A, Lamikiz A, Celaya A. Plasma-assisted milling of heat-resistant superalloys. Journal of Manufacturing Science and Engineering, 2004, 126(2): 274–285
50. Lee Y, Lee C. A study on optimal machining conditions and energy efficiency in plasma-assisted machining of Ti–6Al–4V. Materials, 2019, 12(16): 2590
51. Di L B, Zhang J S, Zhang X L, Wang H Y, Li H, Li Y Q, Bu D C. Cold plasma treatment of catalytic materials: a review. Journal of Physics D: Applied Physics, 2021, 54(33): 333001
52. Rehbinder P. New physico-chemical phenomena in the deformation and mechanical treatment of solids. Nature, 1947, 159(4052): 866–867
53. Chaudhari A, Soh Z Y, Wang H, Kumar A S. Rehbinder effect in ultraprecision machining of ductile materials. International Journal of Machine Tools and Manufacture, 2018, 133: 47–60
54. Yin Q A, Liu Z Q, Wang B. Machinability improvement of Inconel 718 through mechanochemical and heat transfer effects of coated surface-active thermal conductive mediums. Journal of Alloys and Compounds, 2021, 876: 160186
55. Herrera-Jimenez E J, Bousser E, Schmitt T, Klemberg-Sapieha J E, Martinu L. Effect of plasma interface treatment on the microstructure, residual stress profile, and mechanical properties of PVD TiN coatings on Ti–6Al–4V substrates. Surface and Coatings Technology, 2021, 413: 127058
56. Deng Y, Chen W L, Li B X, Wang C Y, Kuang T C, Li Y Q. Physical vapor deposition technology for coated cutting tools: a review. Ceramics International, 2020, 46(11): 18373–18390
57. Meng X F, Zhang K D, Guo X H, Wang C D, Sun L N. Preparation of micro-textures on cemented carbide substrate surface by plasma-assisted laser machining to enhance the PVD tool coatings adhesion. Journal of Materials Processing Technology, 2021, 288: 116870
58. Martinez M A, Abenojar J, Lopez De Armentia S. Environmentally friendly plasma activation of acrylonitrile-butadiene-styrene and polydimethylsiloxane surfaces to improve paint adhesion. Coatings, 2018, 8(12): 428
59. Godec M, Donik Č, Kocijan A, Podgornik B, Skobir Balantič D A. Effect of post-treated low-temperature plasma nitriding on the wear and corrosion resistance of 316L stainless steel manufactured by laser powder-bed fusion. Additive Manufacturing, 2020, 32: 101000
60. Kaseem M, Choe H C. Simultaneous improvement of corrosion resistance and bioactivity of a titanium alloy via wet and dry plasma treatments. Journal of Alloys and Compounds, 2021, 851: 156840
61. Madhavulu G, Ahmed B. Hot machining process for improved metal removal rates in turning operations. Journal of Materials Processing Technology, 1994, 44(3–4): 199–206
62. Kitagawa T, Maekawa K, Kubo A. Plasma hot machining for high hardness metals. Bulletin of the Japan Society of Precision Engineering, 1988, 22(2): 145–151
63. Moon S H, Lee C M. A study on the machining characteristics using plasma-assisted machining of AISI 1045 steel and Inconel 718. International Journal of Mechanical Sciences, 2018, 142–143: 595–602
64. Wang Z Y, Rajurkar K P, Fan J, Lei S, Shin Y C, Petrescu G. Hybrid machining of Inconel 718. International Journal of Machine Tools and Manufacture, 2003, 43(13): 1391–1396
65. Feyzi T, Safavi S M. Improving machinability of Inconel 718 with a new hybrid machining technique. The International Journal of Advanced Manufacturing Technology, 2013, 66(5–8): 1025–1030
66. Leshock C E, Kim J N, Shin Y C. Plasma enhanced machining of Inconel 718: modeling of workpiece temperature with plasma heating and experimental results. International Journal of Machine Tools and Manufacture, 2001, 41(6): 877–897
67. Shao-Hsien C, Tsai K T. Predictive analysis for the thermal diffusion of the plasma-assisted machining of superalloy Inconel-718 based on exponential smoothing. Advances in Materials Science and Engineering, 2018, 2018: 9532394
68. Farahnakian M, Razfar M R. Experimental study on hybrid ultrasonic and plasma aided turning of hardened steel AISI 4140. Materials and Manufacturing Processes, 2014, 29(5): 550–556
69. Sun S, Brandt M, Dargusch M S. Thermally enhanced machining of hard-to-machine materials—a review. International Journal of Machine Tools and Manufacture, 2010, 50(8): 663–680
70. Fitriani S W, Ikeda S, Tani M, Yajima H, Furuta H, Hatta A. Hydrophilization of polytetrafluoroethylene using an atmospheric-pressure plasma of argon gas with water–ethanol vapor. Materials Chemistry and Physics, 2022, 282: 125974
71. Dufour T, Gutierrez Q. Cold plasma treatment of seeds: deciphering the role of contact surfaces through multiple exposures, randomizing and stirring. Journal of Physics D: Applied Physics, 2021, 54(50): 505202
72. Dufour T, Gutierrez Q, Bailly C. Sustainable improvement of seeds vigor using dry atmospheric plasma priming: evidence through coating wettability, water uptake, and plasma reactive chemistry. Journal of Applied Physics, 2021, 129(8): 084902
73. Oehr C, Hegemann D, Liehr M, Wohlfart P. Cost structure and resource efficiency of plasma processes. Plasma Processes and Polymers, 2022, 19(10): 2200022
74. Chiper A S. Tailoring the working gas flow to improve the surface modification of plasma-treated polymers. Materials Letters, 2021, 305: 130832
75. Dvořáková H, Čech J, Stupavská M, Prokeš L, Jurmanová J, Buršíková V, Ráheľ J, Sťahel P. Fast surface hydrophilization via atmospheric pressure plasma polymerization for biological and technical applications. Polymers, 2019, 11(10): 1613

76. Liu J Y, Song J L, Wang G S, Chen F Z, Liu S, Yang X L, Sun J, Zheng H X, Huang L, Jin Z J, Liu X. Maskless hydrophilic patterning of the superhydrophobic aluminum surface by an atmospheric pressure microplasma jet for water adhesion controlling. ACS Applied Materials & Interfaces, 2018, 10(8): 7497–7503
77. Thompson R, Austin D, Wang C, Neville A, Lin L. Low-frequency plasma activation of nylon 6. Applied Surface Science, 2021, 544: 148929
78. Jang H J, Jung E Y, Parsons T, Tae H, Park C. A review of plasma synthesis methods for polymer films and nanoparticles under atmospheric pressure conditions. Polymers, 2021, 13(14): 2267
79. Huang S, Yin S H, Chen F J, Luo H, Tang Q C, Song J L. Directional transport of droplets on wettability patterns at high temperature. Applied Surface Science, 2018, 428: 432–438
80. Chen X D, Qiu H H. Bubble dynamics and heat transfer on a wettability patterned surface. International Journal of Heat and Mass Transfer, 2015, 88: 544–551
81. Qiu Y H, Liu Z H. The theoretical simulation of the effect of solid-liquid contact angle on the critical heat flux of saturated water jet boiling on stagnation zone. International Journal of Heat and Mass Transfer, 2010, 53(9–10): 1921–1926
82. Takata Y, Hidaka S, Cao J M, Nakamura T, Yamamoto H, Masuda M, Ito T. Effect of surface wettability on boiling and evaporation. Energy, 2005, 30(2–4): 209–220
83. Chen R K, Lu M C, Srinivasan V, Wang Z J, Cho H H, Majumdar A. Nanowires for enhanced boiling heat transfer. Nano Letters, 2009, 9(2): 548–553
84. Yamamura K, Takiguchi T, Ueda M, Deng H, Hattori A N, Zettsu N. Plasma-assisted polishing of single crystal SiC for obtaining atomically flat strain-free surface. CIRP Annals-Manufacturing Technology, 2011, 60(1): 571–574
85. Liu J Y, Song J L, Chen Y, Zhang J C, Wu L B, Wang G S, Zhang F, Liu Z A, Sun J, Liu S, Liu X, Jin Z J, Zhao D Y. Atmospheric pressure cold plasma jet-assisted micro-milling TC4 titanium alloy. The International Journal of Advanced Manufacturing Technology, 2021, 112(7–8): 2201–2209
86. Xu W J, Huang S, Chen F Z, Song J L, Liu X. Diamond wear properties in cold plasma jet. Diamond and Related Materials, 2014, 48: 96–103
87. Liu X, Chen F Z, Huang S, Yang X L, Lu Y, Zhou W L, Xu W J. Characteristic and application study of cold atmospheric-pressure nitrogen plasma jet. IEEE Transactions on Plasma Science, 2015, 43(6): 1959–1968
88. Chen F Z, Liu S, Liu J Y, Huang S, Xia G Q, Song J L, Xu W J, Sun J, Liu X. Surface modification of tube inner wall by transferred atmospheric pressure plasma. Applied Surface Science, 2016, 389: 967–976
89. Deng H, Monna K, Tabata T, Endo K, Yamamura K. Optimization of the plasma oxidation and abrasive polishing processes in plasma-assisted polishing for highly effective planarization of 4H-SiC. CIRP Annals-Manufacturing Technology, 2014, 63(1): 529–532
90. Deng H, Yamamura K. Atomic-scale flattening mechanism of 4H-SiC (0001) in plasma-assisted polishing. CIRP Annals-Manufacturing Technology, 2013, 62(1): 575–578
91. Deng H, Yamamura K. Smoothing of reaction sintered silicon carbide using plasma-assisted polishing. Current Applied Physics, 2012, 12: S24–S28
92. Deng H, Ueda M, Yamamura K. Characterization of 4H-SiC (0001) surface processed by plasma-assisted polishing. The International Journal of Advanced Manufacturing Technology, 2014, 72(1–4): 1–7
93. Yamamura K, Takiguchi T, Ueda M, Hattori A N, Zettsu N. High-integrity finishing of 4H-SiC (0001) by plasma-assisted polishing. Advanced Materials Research, 2010, 126–128: 423–428
94. Deng H, Ueda M, Yamamura K. Chemical and morphological analysis of 4H-SiC surface processed by plasma-assisted polishing. Key Engineering Materials, 2012, 516: 186–191
95. Sun R Y, Yang X, Arima K, Kawai K, Yamamura K. High-quality plasma-assisted polishing of aluminum nitride ceramic. CIRP Annals-Manufacturing Technology, 2020, 69(1): 301–304
96. Sun R Y, Nozoe A, Nagahashi J, Arima K, Kawai K, Yamamura K. Novel highly-efficient and dress-free polishing technique with plasma-assisted surface modification and dressing. Precision Engineering, 2021, 72: 224–236
97. Deng H, Endo K, Yamamura K. Plasma-assisted polishing of gallium nitride to obtain a pit-free and atomically flat surface. CIRP Annals-Manufacturing Technology, 2015, 64(1): 531–534
98. Yamamura K, Emori K, Sun R, Ohkubo Y, Endo K, Yamada H, Chayahara A, Mokuno Y. Damage-free highly efficient polishing of single-crystal diamond wafer by plasma-assisted polishing. CIRP Annals-Manufacturing Technology, 2018, 67(1): 353–356
99. Luo H, Ajmal K M, Liu W, Yamamura K, Deng H. Atomic-scale and damage-free polishing of single crystal diamond enhanced by atmospheric pressure inductively coupled plasma. Carbon, 2021, 182: 175–184
100. Liu N, Sugawara K, Yoshitaka N, Yamada H, Takeuchi D, Akabane Y, Fujino K, Kawai K, Arima K, Yamamura K. Damage-free highly efficient plasma-assisted polishing of a 20-mm square large mosaic single crystal diamond substrate. Scientific Reports, 2020, 10(1): 19432
101. Liu N, Sugimoto K, Yoshitaka N, Yamada H, Sun R Y, Kawai K, Arima K, Yamamura K. Effects of polishing pressure and sliding speed on the material removal mechanism of single crystal diamond in plasma-assisted polishing. Diamond and Related Materials, 2022, 124: 108899
102. Bastawros A F, Chandra A, Poosarla P A. Atmospheric pressure plasma enabled polishing of single crystal sapphire. CIRP Annals-Manufacturing Technology, 2015, 64(1): 515–518
103. Lyu P, Lai M, Liu Z, Fang F Z. Damage-free finishing of Lu_2O_3 by combining plasma-assisted etching and low-pressure polishing. CIRP Annals-Manufacturing Technology, 2022, 71(1): 169–172
104. Koinuma H, Ohkubo H, Hashimoto T, Inomata K, Shiraishi T, Miyanaga A, Hayashi S. Development and application of a microbeam plasma generator. Applied Physics Letters, 1992, 60(7): 816–817
105. Liu L J, Zhang Y, Tian W J, Meng Y, Ouyang J T. Electrical characteristics and formation mechanism of atmospheric pressure

plasma jet. Applied Physics Letters, 2014, 104(24): 244108
106. Algwari Q T, O'Connell D. Electron dynamics and plasma jet formation in a helium atmospheric pressure dielectric barrier discharge jet. Applied Physics Letters, 2011, 99(12): 121501
107. Shao X J, Jiang N, Zhang G J, Cao Z X. Comparative study on the atmospheric pressure plasma jets of helium and argon. Applied Physics Letters, 2012, 101(25): 253509
108. Matsusaka S. Control of particle charge by atmospheric pressure plasma jet (APPJ): a review. Advanced Powder Technology, 2019, 30(12): 2851–2858
109. Cheng H, Liu X, Lu X P, Liu D W. Numerical study on propagation mechanism and bio-medicine applications of plasma jet. High Voltage, 2016, 1(2): 62–73
110. Jiang N, Ji A L, Cao Z X. Atmospheric pressure plasma jet: effect of electrode configuration, discharge behavior, and its formation mechanism. Journal of Applied Physics, 2009, 106(1): 013308
111. Latham J, Belova E V, Yamada M. Numerical study of coronal plasma jet formation. Physics of Plasmas, 2021, 28(1): 012901
112. Yu N, Yang Y N, Jourdain R, Gourma M, Bennett A, Fang F Z. Design and optimization of plasma jet nozzles based on computational fluid dynamics. The International Journal of Advanced Manufacturing Technology, 2020, 108(7–8): 2559–2568
113. Takemura Y, Kubota Y, Yamaguchi N, Hara T. Development of atmospheric plasma jet with long flame. IEEE Transactions on Plasma Science, 2009, 37(8): 1604–1606
114. Johnson M J, Boris D R, Petrova T B, Walton S G. Characterization of a compact, low-cost atmospheric-pressure plasma jet driven by a piezoelectric transformer. IEEE Transactions on Plasma Science, 2019, 47(1): 434–444
115. Zhu P, Li B, Duan Z C, Ouyang J T. Development from dielectric barrier discharge to atmospheric pressure plasma jet in helium: experiment and fluid modeling. Journal of Physics D: Applied Physics, 2018, 51(40): 405202
116. Liu W Z, Zheng Q T, Hu M C, Zhao L X, Li Z Y. Study of generation characteristics of glow-type atmospheric-pressure plasma jet based on DC discharge in air. Plasma Science & Technology, 2019, 21(12): 125404
117. Srakaew K, Chingsungnoen A, Sutthisa W, Lakhonchai A, Poolcharuansin P, Chunpeng P, Rojviriya C, Thumanu K, Tunmee S. Development of a multihole atmospheric plasma jet for growth rate enhancement of broccoli seeds. Processes, 2021, 9(7): 1134
118. Fu W J, Zhang C Y, Nie C, Li X Y, Yan Y. A high efficiency low-temperature microwave-driven atmospheric pressure plasma jet. Applied Physics Letters, 2019, 114(25): 254106
119. Liu X. Basic research on mechanism and application of ionized gas jet assisted cutting. Dissertation for the Doctoral Degree. Dalian: Dalian University of Technology, 2012, 131–134 (in Chinese)
120. Xu W J, Liu X, Song J L, Wu L B, Sun J. Friction and wear properties of Ti6Al4V/WC-Co in cold atmospheric plasma jet. Applied Surface Science, 2012, 259: 616–623
121. Huang S, Liu X, Chen F Z, Zheng H X, Yang X L, Wu L B, Song J L, Xu W J. Diamond-cutting ferrous metals assisted by cold plasma and ultrasonic elliptical vibration. The International Journal of Advanced Manufacturing Technology, 2016, 85(1–4): 673–681
122. Tang Q C, Yin S H, Chen F J, Huang S, Luo H. New technology for cutting ferrous metal with diamond tools. Diamond and Related Materials, 2018, 88: 32–42
123. Liu X, Zhang F, Liu J Y, Zhang J C, Chen Y, Zhang Z T, Shen H Y, Kong J X, Sun J. Atmospheric pressure plasma-assisted precision turning of pure iron material. The International Journal of Advanced Manufacturing Technology, 2020, 106(11–12): 5187–5197
124. Liu J Y, Chen Y, Zhang J C, Wu L B, Yang Z K, Zhang F, Sun J, Liu X, Jin Z J, Zhao D Y. Atmospheric pressure plasma jet and minimum quantity lubrication assisted micro-grinding of quenched GCr15. The International Journal of Advanced Manufacturing Technology, 2020, 106(1–2): 191–199
125. Mustafa G, Liu J Y, Zhang F, Wang G S, Yang Z K, Harris M, Liu S, Liu X, Jin Z J, Sun J. Atmospheric pressure plasma jet assisted micro-milling of Inconel 718. The International Journal of Advanced Manufacturing Technology, 2019, 103(9–12): 4681–4687